

Necrostatin-1 decreases necroptosis and inflammatory markers after intraventricular hemorrhage in mice

<https://doi.org/10.4103/1673-5374.339488>

Date of submission: June 29, 2021

Date of decision: October 20, 2021

Date of acceptance: January 20, 2022

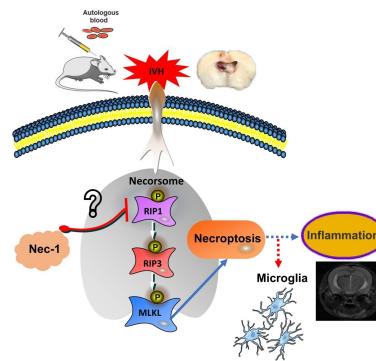
Date of web publication: April 29, 2022

Chang Liu^{1, #}, Yi Cao^{2, #}, Hao-Xiang Wang¹, Long Zhao^{1, 3}, Ya-Xing Chen¹, Kun-Hong Zhong⁴, Gao-Wei Li¹, Guo-Qing Wang¹, Ke-Ru Huang¹, Ai-Ping Tong^{4, *}, Liang-Xue Zhou^{1, *}

From the Contents

Introduction	2710
Materials and Methods	2710
Results	2711
Discussion	2713

Graphical Abstract Mechanism of necroptosis after intraventricular hemorrhage



Abstract

Necrostatin-1, an inhibitor of necroptosis, can effectively inhibit necrotic apoptosis in neurological diseases, which results in the inhibition of inflammation, endoplasmic reticulum stress, and reactive oxygen species production and substantial improvement of neurological function. However, the effects of necrostatin-1 on intraventricular hemorrhage (IVH) remain unknown. In this study, we established a mouse model of IVH by injecting autologous blood into the lateral ventricle of the brain. We also injected necrostatin-1 into the lateral ventricle one hour prior to IVH induction. We found that necrostatin-1 effectively reduced the expression levels of the necroptosis markers receptor-interacting protein kinase (RIP)1, RIP3, mixed lineage kinase domain-like protein (MLKL), phosphorylated (p)-RIP3, and p-MLKL and the levels of interleukin-1 β , interleukin-6, and tumor necrosis factor- α in the surrounding areas of the lateral ventricle. However, necrostatin-1 did not reduce ependymal ciliary injury or brain water content. These findings suggest that necrostatin-1 can prevent local inflammation and microglial activation induced by IVH but does not greatly improve prognosis.

Key Words: ependymal cilia; hydrocephalus; inflammation; intraventricular hemorrhage; microglia; MLKL; necroptosis; necrostatin-1; RIP1; RIP3

Introduction

Intraventricular hemorrhage (IVH) is a common neurological disorder with a high mortality rate (Hanley et al., 2017; Bosche et al., 2020). In adults, IVH is often secondary to physical brain trauma, hypertensive intracerebral hemorrhage (ICH), or subarachnoid hemorrhage (Jabbarli et al., 2016; Moullaali et al., 2017; Kowalski et al., 2021). In preterm infants, IVH is usually caused by germinal matrix hemorrhage adjacent to the lateral ventricle (Segado-Arenas et al., 2018). When the combination occurs, it is known as germinal matrix hemorrhage-IVH, which occurs in approximately three per 1000 live births and has a mortality rate of 20–30% in the USA (Klebe et al., 2020). Researchers have found that certain treatments, such as celecoxib and minocycline, can improve the prognosis of IVH in animals, and these studies may lead to promising treatments for IVH patients (Ko et al., 2018; Ballabh and de Vries, 2021). At present, there are no in-depth studies on the pathogenesis and development of IVH and secondary injuries. Therefore, it is critical to clarify the pathological mechanism of brain injury after IVH and design effective intervention measures to improve the clinical prognosis of IVH patients.

Necroptosis is a type of programmed cell death that was discovered recently. Necroptosis is a caspase-independent mode of cell death that is mediated by death receptors and results in morphological changes that are characteristic of necrotic cells (Yuan et al., 2019a). The formation of a necrotic death complex (necrosome), which includes receptor-interacting protein kinase 1 (RIP1), receptor-interacting protein kinase 3 (RIP3), and mixed lineage

kinase domain-like protein (MLKL), plays a critical role in necroptosis, and deregulation of necroptosis is associated with pathological conditions in various systems, including inflammatory diseases (Wallach et al., 2016). Evidence has emerged that suggests necroptosis is involved in various neurological diseases (Caccamo et al., 2017; Morrice et al., 2017; Naito et al., 2020). Necrostatin-1 (Nec-1), a small molecule compound, inhibits the activity of RIP1 and is a specific inhibitor of necroptosis (Degterev et al., 2005). RIP3 and MLKL are key proteins involved in the process of necroptosis. A large number of animal experiments have shown that Nec-1 can effectively inhibit necroptosis in neurological diseases, thereby inhibiting inflammation, endoplasmic reticulum stress, production of reactive oxygen species and significantly improving neurological function (Liang et al., 2019; Cao and Mu, 2021). However, it remains unknown whether necroptosis occurs during IVH and whether Nec-1 may be neuroprotective under this condition. In this study, we investigated whether necroptosis occurs in the periventricular tissue after IVH using a mouse model. In addition, we evaluated the potential protective effects of the necroptosis inhibitor Nec-1 during IVH.

Materials and Methods

Animals

Estrogen has a neuroprotective effect on intracerebral hemorrhage-related diseases (Ding et al., 2014), which may have influenced the results of this study. Therefore, a total of 165 male C57BL/6 mice (weighing 23–27 g, 7–9 weeks of age, special pathogen-free level) were purchased from the

¹Department of Neurosurgery, West China Medical School, West China Hospital, Sichuan University, Chengdu, Sichuan Province, China; ²Department of Neurosurgery, Chengdu Second People's Hospital, Chengdu, Sichuan Province, China; ³Department of Neurosurgery, Affiliated Hospital of North Sichuan Medical College, Nanchong, Sichuan Province, China; ⁴State Key Laboratory of Biotherapy, West China Medical School, Sichuan University, Chengdu, Sichuan Province, China

*Correspondence to: Liang-Xue Zhou, MD, zhxlxl@163.com; Ai-Ping Tong, MD, aipingtong@scu.edu.cn.
<https://orcid.org/0000-0001-9991-6358> (Liang-Xue Zhou); <https://orcid.org/0000-0002-1782-399X> (Chang Liu)
#Both authors contributed equally to this work.

Funding: The work was funded by Major National Science and Technology Projects, China, No. 2019ZX09301-147 (to LXZ); and Postdoctoral Foundation of West China Hospital of Sichuan University, China, No. 2020HXBH160 (to YXC).

How to cite this article: Liu C, Cao Y, Wang HX, Zhao L, Chen YX, Zhong KH, Li GW, Wang GQ, Huang KR, Tong AP, Zhou LX (2022) Necrostatin-1 decreases necroptosis and inflammatory markers after intraventricular hemorrhage in mice. *Neural Regen Res* 17(12):2710-2716.

Laboratory Animal Center of Sichuan University (license No. SCXK [Chuan] 2018-026). All mice were housed in a room with 25°C and humidity control, under a 12-hour light/dark cycle and free to access food and water. All procedures were conducted strictly in accordance with the animal use procedures approved by the Sichuan University Animal Protection and Use Committee on April 15, 2020. All experiments were designed and reported in accordance with the Animal Research: Reporting of *In Vivo* Experiments (ARRIVE) guidelines (Percie du Sert et al., 2020).

Intracerebroventricular injection

The animals were randomly divided into three groups: sham ($n = 51$), IVH ($n = 78$), and IVH + Nec-1 ($n = 36$) groups. The IVH model was established by injecting fresh autologous blood into a lateral ventricle of the brain using a stereotaxic frame (RWD; Shenzhen, China). In brief, the mice were anesthetized by intraperitoneal injection of 2% pentobarbital sodium (Sigma; St. Louis, MO, USA) and then secured in the stereotaxic frame. A burr hole was drilled in the skull through which a needle was inserted into the lateral ventricle at the following stereotaxic coordinates: 0.5 mm posterior to the bregma, 1.5 mm lateral of the bregma, and 2.2 mm in depth. Then, the tail of each mouse was cut, and 50 μ L of fresh autologous blood was collected. The autologous blood (50 μ L) was injected into the lateral ventricle within 10 minutes using a microsyringe. After injection, the needle position was maintained for 5 minutes. Finally, the microsyringe was removed, and the hole was sealed with bone wax. Mice in the sham group only received scalp resection.

Nec-1 intervention

Nec-1 (Selleck; Houston, TX, USA) was diluted with dimethyl sulfoxide (Sigma) to a concentration of 2.6 μ g/ μ L. For the IVH + Nec-1 group, 1 μ L Nec-1 (2.6 μ g) solution was administered into the single lateral ventricle (co-ordinates relative to the bregma: 0.5 mm anterior to the bregma, 1.5 mm lateral of the bregma, and 2.2 mm in depth) one hour prior to IVH induction. Animals that died were excluded from the study.

Western blot analysis

Mice were anesthetized with pentobarbital sodium, the hearts were perfused with phosphate-buffered saline (PBS), and the brains were collected 3 days after IVH induction. Samples were extracted from the periventricular tissue of the hemorrhagic side of the brain. The brain tissue was placed in a centrifuge tube, lysis buffer was added, and the tissue was crushed on ice using an ultrasonic comminution instrument (Shunma, Nanjing, China). The tissue was placed on ice for 30 minutes and centrifuged at 12,000 r/min at 4°C for 20 minutes. After approximately two hours of electrophoresis, the proteins were transferred to polyvinylidene fluoride membranes (Millipore, Billerica, MA, USA), which were blocked with 5% skim milk or bovine serum albumin at room temperature for 1 hour. The samples were incubated with the following primary antibodies at 4°C overnight: anti-RIP3 rabbit; (1:600; Huabio, Hangzhou, China, Cat# ER1901-27), anti-MLKL (rabbit; 1:500; Millipore, Cat# SAB5700808), anti-RIP1 (mouse; 0.5 μ g/mL; R and D Systems, Minneapolis, MN, USA, Cat# MAB3585-SP, RRID: AB_2253447), anti-interleukin (IL)-1 β (rabbit; 1:1000; Abcam, Cambridge, UK, Cat# ab254360, RRID: AB_598195), anti-IL-6 (rabbit; 1:1000; Abcam, Cat# ab229381, RRID: AB_2861234), anti-tumor necrosis factor (TNF)- α (rabbit; 1:1000; Abcam, Cat# ab183218, RRID: AB_2889388), and anti- β -actin (mouse; 1:2000; Servicebio, Wuhan, China, Cat# GB12001). The secondary antibodies were horseradish peroxidase-conjugated affinitypure goat anti-rabbit IgG (H+L) (1:5000; Proteintech, Wuhan, China, Cat# SA00001-2, RRID: AB_2722564) and horseradish peroxidase-conjugated affinitypure goat anti-mouse IgG (H+L) (1:5000; Proteintech, Cat# SA00001-1, RRID: AB_2722565). After incubation with the secondary antibody at room temperature for 1 hour, the protein bands were detected using electrochemiluminescence substrate (Solarbio). ImageJ software (Version 7.4; National Institutes of Health, Bethesda, MD, USA) (Schneider et al., 2012) was used to calculate the gray value ratio of the target band/ β -actin.

Immunohistochemistry and immunofluorescent staining

For immunohistochemistry, the hearts of the mice were perfused with PBS on day 3 after modeling followed by paraformaldehyde, and the brain tissues were removed and fixed in paraformaldehyde. After dehydration, the tissue was paraffin-embedded and sections were prepared. The brain tissue sections were dewaxed and immersed in sodium citrate for 25 minutes at 95°C. Peroxidase inhibition was achieved by incubating the tissue sections with 0.3% hydrogen peroxide for 15 minutes. The sections were incubated with anti-phosphorylated (p)-RIP3 (1:100; rabbit; Abcam, Cat# ab195117, RRID: AB_2768156) and anti-p-MLKL (1:100; rabbit; Abcam, Cat# ab196436, RRID: AB_2687465) antibodies at 4°C overnight. Subsequently, the sections were stained using an immunohistochemistry kit (PV9000 kit; ZSGB-BIO, Beijing, China) following the manufacturer's instructions and sealed prior to observation. For immunofluorescence, sections were blocked with goat serum (Boster, Wuhan, China) for 1 hour at room temperature and incubated overnight at 4°C with one of the following primary antibodies against: p-RIP3 and p-MLKL (described above), neuronal nuclei antigen (5 μ g/mL; mouse; Abcam, Cat# ab104224, RRID: AB_10711040), glial fibrillary acidic protein (1:500; Servicebio; mouse; Cat# GB12096), ionized calcium binding adapter molecule 1 (Iba-1; 1:1000; rabbit; FUJIFILM Wako Shibayagi, Cat# 016-26721, RRID: AB_2811160 or 1:500; Servicebio; mouse; Cat# GB12105), and IL-6 (1:50; rabbit; Cat# GB11117, Servicebio). Then, the tissue sections were incubated with the secondary antibodies Coralite488-conjugated affinitypure goat anti-mouse IgG (H+L) (1:100; Proteintech, Cat# SA00013-1, RRID: AB_2810983), Coralite488-conjugated affinitypure goat anti-rabbit IgG(H+L) (1:100; Proteintech, Cat# SA00013-2, RRID: AB_2797132), or Coralite594-

conjugated goat anti-rabbit IgG (H+L) (1:100; Proteintech, Cat# SA00013-4, RRID: AB_2810984) at room temperature for 2 hours followed by incubation with 2-(4-amidinophenyl)-6-indolecarbamidine dihydrochloride (Thermo Fisher Scientific) for 5 minutes. The sections were sealed and observed with a fluorescence microscope (Zeiss, Jena, Germany). The results were presented as relative fluorescence intensity.

Propidium iodide and hematoxylin-eosin staining

For propidium iodide (PI) staining, on day 3 after IVH induction, PI staining solution (Sigma) was diluted with sterile normal saline to a concentration of 10 mg/mL. PI solution (1 μ L) was injected into the lateral ventricle (right side) of each mouse one hour prior to euthanasia with 2% pentobarbital sodium. The brain tissue was removed and frozen sections were prepared. The sections were incubated with 2-(4-amidinophenyl)-6-indolecarbamidine dihydrochloride prior to observation with a fluorescence microscope. For hematoxylin-eosin (HE) staining, paraffin-embedded sections were dewaxed, and coronal sections of the brain tissue were stained with hematoxylin solution (Servicebio) for 5 minutes followed by treatment with hematoxylin differentiation solution. Finally, the sections were dyed with eosin (Servicebio) for 5 minutes. The sections were dehydrated and sealed, and the images were collected using optical microscopy (BX53F; Olympus; Tokyo, Japan).

Magnetic resonance imaging

For detecting secondary hydrocephalus on day 3 after modeling, mice were anesthetized by inhalation of 2% isoflurane (RWD) and subjected to magnetic resonance imaging (MRI). A 7.0-Tesla MR scanner (Bruker; Karlsruhe, Germany) with a T2 fast spin echo sequence (matrix, 256 \times 256; echo time, 2.5 ms; repetition time, 100 ms) was used for image acquisition of mouse heads. A total of 18 coronal slices were obtained for each scan with a view field of 35 mm \times 35 mm and slice thickness of 1.0 mm.

Scanning electron microscopy

On day 3 after modeling, mice were anesthetized with pentobarbital sodium and the brains were collected after heart perfusion with PBS. Coronal sections (1 mm thick) were prepared, and the tissue containing the lateral ventricle wall was separated and immersed in electron microscope fixative solution (Servicebio). Tissue blocks were washed three times for 15 minutes each and transferred to a 1% osmium tetroxide solution for 2 hours. Tissue blocks were washed three times for 15 minutes each. The samples were placed on the metal stub with a carbon sticker, and the gold foil was sprayed for 30 minutes. Finally, tissue samples were observed, and images were captured with a scanning electron microscope (SU8100; Hitachi; Tokyo, Japan).

Brain water content measurement

On day 3 after modeling, mice were anesthetized with pentobarbital sodium, and their intact brains were removed and placed on pre-weighed and numbered tin foil paper. Wet tissues were weighed on an electronic balance (Sartorius; Göttingen, Germany). After drying the tissue for 72 hours at 100°C, the dry weights were measured. The formula for calculating brain water content was as follows: (wet weight – dry weight)/wet weight \times 100%.

Quantitative reverse transcription-polymerase chain reaction

Total RNA was extracted from periventricular tissue 3 days after IVH induction. Quantitative reverse transcription-polymerase chain reaction (qRT-PCR) was performed after reverse transcription. The primers used were as follows: *Rip3*: forward, 5'-CCA GAG AGC CAA GCC AAA GAG-3'; reverse, 5'-AGC CAC GGG GTC AGA AGA TG-3'; *Mkl1*: forward, 5'-CCC ATT TGA AGG CTG TGA TTC TAA G-3'; reverse, 5'-CAG AAA GAC TCC TAC CGT CCA CA-3'; *Gapdh*: forward, 5'-CCT CGT CCT GGA GAC AAA ATG-3'; reverse, 5'-TGA GGT CAA TGA AGG GGT CGT-3'. The results were calculated using the $\Delta\Delta$ CT method (Tabatabaieian and Hojati, 2013).

Statistical analysis

GraphPad Prism software (version 6.01; GraphPad; San Diego, CA, USA, www.graphpad.com) was used for statistical analysis. All data are presented as the mean \pm standard error of mean (SEM). Statistical differences among groups were analyzed using unpaired Student's *t*-tests, and statistical significance was set at $P < 0.05$.

Results

The IVH model was successfully established and necroptosis occurred in the periventricular tissues after IVH induction

We established a mouse IVH model by injecting 50 μ L of autologous blood into the ventricles to investigate whether necroptosis occurred after IVH induction (Figure 1A). Brain tissue sections demonstrated that blood was present in the lateral ventricles at all levels, and the blood was observed in the gap between the hippocampus and corpus callosum (Figure 1B). T2-weighted MRI images revealed that low signals were present in the lateral ventricles 1 day after IVH induction (Figure 1C). Furthermore, we chose days 1, 3, 5, and 7 after IVH modeling as the time points to observe changes in expression of the necroptosis markers RIP3 and MLKL. Western blots showed that the expression of RIP3 and MLKL in the periventricular tissues was highest on day 3 after IVH modeling compared with expression in the sham group ($P < 0.01$; Figure 2A–C). In addition, immunohistochemistry demonstrated that positive staining for p-RIP3 and p-MLKL within the periventricular tissues increased by day 3 after IVH induction compared with that in the sham group ($P < 0.01$; Figure 2D–G). These results indicated that necroptosis occurred in the area of the lateral ventricle after IVH was induced and was predominant on day 3 after IVH modeling.

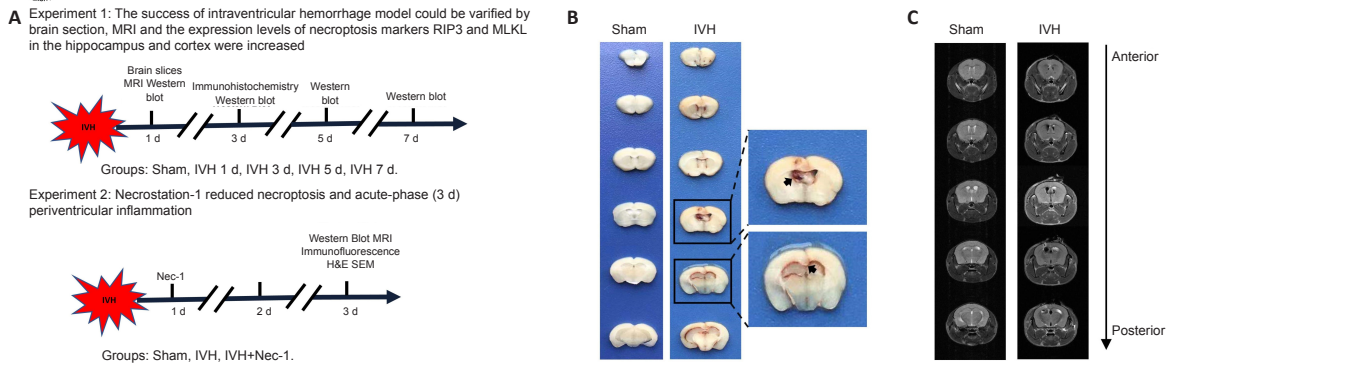


Figure 1 | Experimental design and establishment of the IVH model.

(A) Experimental design and animal groups. (B) Brain tissue sections from mice in the sham and IVH groups 1 day after modeling. The ventricle size in the sham group was normal. In the IVH group, the obvious presence of blood was observed in the ventricular system at all levels. The arrows indicate the blood in the brain tissue. (C) T2-weighted MRI of brains from the sham and IVH groups 1 day after modeling. In the sham group, the ventricular system was filled with normal cerebrospinal fluid, and T2 images presented a high signal. In the IVH group, the T2 images of the ventricular system demonstrated a low signal, indicating blood retention in the ventricle. H&E: Hematoxylin-eosin staining; IVH: intraventricular hemorrhage; MRI: magnetic resonance imaging; Nec-1: necrostatin-1; SEM: scanning electron microscope.

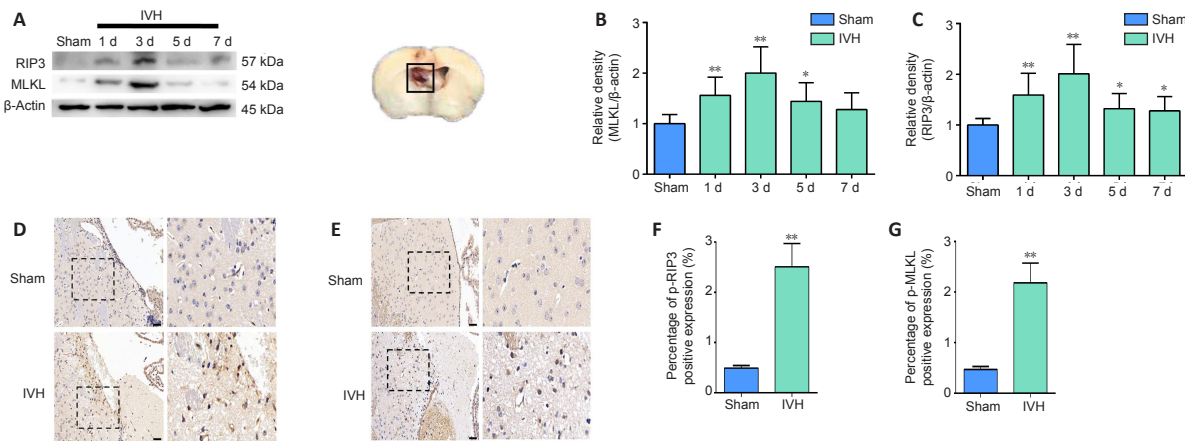


Figure 2 | Changes in levels of necroptosis markers within the periventricular tissue after IVH induction.

(A) Representative western blots of RIP3 and MLKL. The box represents the tissue-extraction site for western blot assay. (B, C) Quantitative analyses of RIP3 (B) and MLKL (C) protein levels. (D, E) Representative images of immunostaining for p-RIP3 (D) and p-MLKL (E) in the sham and IVH groups on day 3 post-IVH induction. No significant positive results were observed for p-RIP3 or p-MLKL in the sham group, while p-RIP3 and p-MLKL were expressed in the IVH group. Scale bars: 50 μ m. (F, G) Statistical analysis of p-RIP3 (F) and p-MLKL (G) expression in tissue from the sham and IVH groups on day 3. Data are expressed as the mean \pm SEM ($n = 6$). * $P < 0.05$, ** $P < 0.01$, vs. sham group (unpaired Student's t -test). IVH: Intraventricular hemorrhage; MLKL: mixed lineage kinase domain-like protein; Nec-1: necrostatin-1; p-MLKL: phosphorylation mixed lineage kinase domain-like protein; p-RIP3: phosphorylation receptor-interacting protein 3; RIP3: receptor-interacting protein 3.

Spatial expression of p-RIP3 and p-MLKL in periventricular tissues 3 days after IVH induction

To determine the cellular localization of activated RIP3 and MLKL 3 days after IVH induction, we used immunofluorescence to observe which types of cells expressed p-RIP3 and p-MLKL. We found that the necroptosis markers p-RIP3 and p-MLKL were mainly expressed in neurons and rarely co-localized with astrocytes or microglia after IVH modeling (Figure 3A and B, respectively).

Nec-1 reduced the expression of necroptosis markers in periventricular tissues on day 3 after IVH induction

We found that RIP1 expression increased after IVH ($P < 0.01$, vs. sham group), and the expression level of RIP1 in the IVH + Nec-1 group was lower than that in the IVH group ($P < 0.01$; Figure 4A and B). Moreover, we used immunofluorescent staining and qRT-PCR to determine the effect of Nec-1 on necroptosis after IVH. The fluorescence intensity for p-RIP3 and p-MLKL and the mRNA expression of Rip3 and Mkl were upregulated in the IVH group ($P < 0.05$ vs. sham group), but the addition of Nec-1 attenuated these changes ($P < 0.05$ or $P < 0.01$, vs. IVH group; Figure 4C–H).

Nec-1 did not significantly alleviate periventricular injury 3 days after IVH induction

The number of PI-positive cells in the periventricular tissue from mice in the IVH group increased compared with that in the sham group ($P < 0.01$). Pretreatment with Nec-1 reduced the number of PI-positive cells compared with that in the IVH only group ($P < 0.05$; Figure 5A and B). The HE staining results showed ependymal wall disruption and cell denudation in the tissue from the IVH group, and there were almost no intact ependymal cilia by general observation. Nec-1 treatment did not significantly alleviate periventricular injury or damage to ependymal cilia induced by IVH (Figure 5C).

Nec-1 decreased microglial activation and expression of inflammatory factors in the tissue surrounding the lateral ventricle 3 days after IVH

Changes in microglia levels were observed with immunofluorescent staining. The numbers of Iba1-positive cells were increased in the area of the lateral ventricles after IVH induction compared with that in the sham group. Moreover, fewer Iba1-positive cells were noted around the lateral ventricle in the IVH + Nec-1 group than that in the IVH group ($P < 0.01$; Figure 6A and B). In addition, we selected IL-1 β , IL-6, and TNF- α as markers to assess the effect of Nec-1 on inflammatory factors after IVH. Immunofluorescent staining of IL-6 was performed to determine whether Nec-1 demonstrated an anti-neuroinflammatory effect after IVH. While the relative fluorescent intensity of IL-6 was increased after IVH induction, Nec-1 treatment partially reversed this effect ($P < 0.01$, vs. IVH group; Figure 6C and D). Western blots showed that the expression of the three inflammatory factors was increased in the IVH group compared with that in the sham group ($P < 0.01$), and Nec-1 treatment attenuated the expression of these inflammatory markers ($P < 0.05$, vs. IVH group; Figure 6E–H).

Nec-1 did not improve hydrocephalus after IVH induction

We found that there was obvious hydrocephalus 3 days after IVH modeling by using T2-weighted MRI. However, Nec-1 treatment did not reduce the degree of hydrocephalus (Figure 7A). In addition, we found that Nec-1 treatment did not significantly reduce water content in the brains when compared with that in the IVH only group (Figure 7B). Injury to the ependymal cilia is closely associated with the development of hydrocephalus. We observed the ependymal cilia using scanning electron microscopy. In the IVH group, the ependymal cilia were kinked, disorganized, and there was progressive loss. Nec-1 treatment did not reverse this effect (Figure 7C). Collectively, these results suggested that inhibiting necroptosis in the early stage after IVH may have a limited effect on the formation of secondary hydrocephalus.

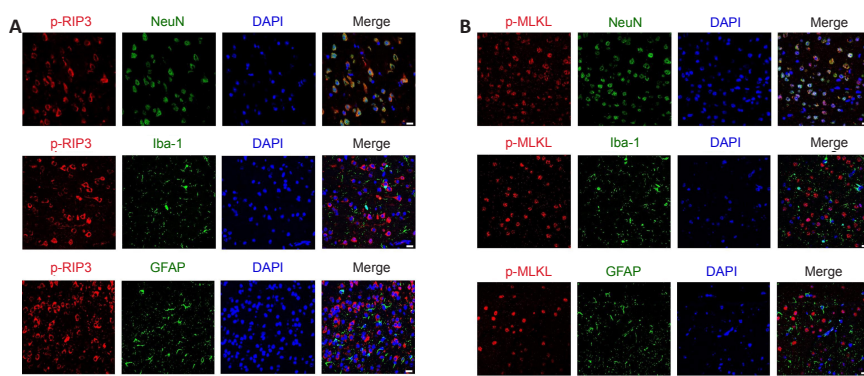


Figure 3 | Immunofluorescent staining for the necroptosis markers p-RIP3 and p-MLKL in the periventricular tissue on day 3 after IVH.

(A) Representative images after immunofluorescent staining for p-RIP3 (red, CoraLite594), NeuN (green, CoraLite488), Iba1 (green, CoraLite488), and GFAP (green, CoraLite488) in the periventricular tissue after IVH. Three days after IVH modeling, the necroptosis indicator p-RIP3 was mainly co-localized with neurons in the lateral ventricle tissue. (B) Representative images after immunofluorescent staining for p-MLKL (red, CoraLite594), NeuN (green, CoraLite488), Iba1 (green, CoraLite488), and GFAP (green, CoraLite488) in the periventricular tissue. Three days after IVH modeling, the necroptosis indicator p-MLKL in the lateral ventricle tissue was mainly co-localized with neurons. Scale bars: 20 μ m. DAPI: 4',6-Diamidino-2-phenylindole; GFAP: glial fibrillary acidic protein; Iba-1: ionized calcium binding adapter molecule 1; IVH: intraventricular hemorrhage; NeuN: neuronal nuclei antigen; p-MLKL: phosphorylation mixed lineage kinase domain-like protein; p-RIP3: phosphorylation receptor-interacting protein 3.

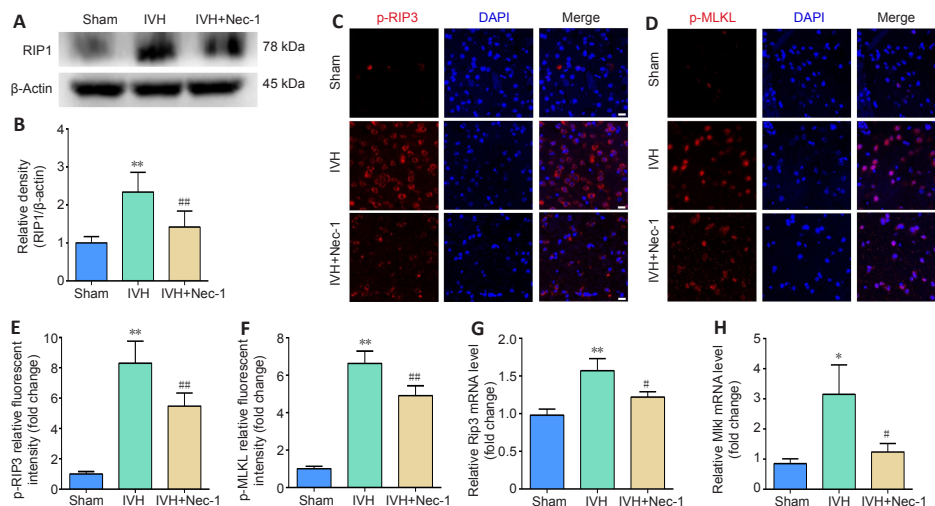


Figure 4 | Effects of necrostatin-1 on the expression of necroptosis markers in periventricular tissue 3 days after IVH induction.

(A) Representative western blot of RIP1. (B) Quantitative analysis of RIP1 protein expression. (C, D) Representative images of p-RIP3 (C; red, CoraLite594) and p-MLKL (D; red, CoraLite594) immunofluorescent staining in the periventricular tissue after IVH. Compared with that in the sham group, p-RIP3 and p-MLKL were significantly increased in the IVH group. Nec-1 attenuated the IVH-mediated increases in p-RIP3 and p-MLKL. Scale bars: 20 μ m. (E, F) Quantitative analyses of p-RIP3 (E) and p-MLKL (F) relative fluorescent intensities in the periventricular tissue. (G, H) qRT-PCR analyses of Rip3 (G) and Mkl1 (H) mRNA expression. Data are expressed as the mean \pm SEM ($n = 3-6$). * $P < 0.05$, ** $P < 0.01$, vs. sham group; # $P < 0.05$, ## $P < 0.01$, vs. IVH group (unpaired Student's *t*-test). DAPI: 4',6-Diamidino-2-phenylindole; IVH: intraventricular hemorrhage; MLKL: mixed lineage kinase domain-like protein; Nec-1: necrostatin-1; p-MLKL: phosphorylation mixed lineage kinase domain-like protein; p-RIP3: phosphorylation receptor-interacting protein 3; qRT-PCR: quantitative reverse transcription-polymerase chain reaction; RIP3: receptor-interacting protein 3.

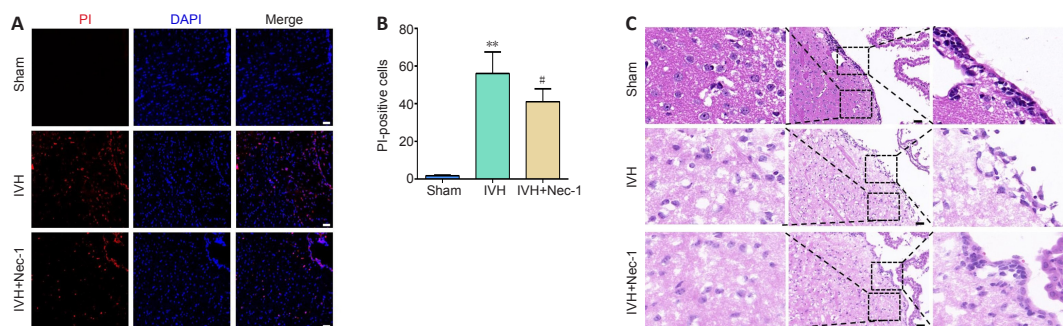


Figure 5 | Effects of necrostatin-1 on necrotic cell death and pathological damage in the periventricular tissue on day 3 after IVH induction.

(A) Representative images of PI (red) staining. Compared with that in the sham group, the numbers of PI-positive cells in the IVH group were increased. Compared with that in the IVH group, the numbers of PI-positive cells in the IVH + Nec-1 group were decreased. Scale bars: 50 μ m. (B) The changes in the number of PI-positive cells in the periventricular tissue. Data are expressed as the mean \pm SEM ($n = 6$). ** $P < 0.01$, vs. sham group; # $P < 0.05$, vs. IVH group (unpaired Student's *t*-test). (C) Representative HE-stained images of the periventricular tissue. In the sham group, the morphology of the periventricular tissue was normal, and the ependymal membrane and cilia were intact. The IVH group showed damage of the periventricular tissue and destruction of the ependymal cilia, while the IVH + Nec-1 group showed no significant improvement in periventricular tissue damage or repair of ependymal cilia. Scale bars: 50 μ m. DAPI: 4',6-Diamidino-2-phenylindole; IVH: intraventricular hemorrhage; Nec-1: necrostatin-1; PI: propidium iodide.

Discussion

Necroptosis is widespread in various neurological diseases. However, it is currently unclear whether necroptosis occurs after IVH. The present study revealed three major findings: (1) necroptosis occurred in the mouse model of IVH, and the expression level of necroptosis markers reached a peak on day 3 after modeling; (2) the key markers of necroptosis, p-RIP3 and p-MLKL, were mainly expressed in neurons and Nec-1 administration reduced the expression of RIP1, p-RIP3, RIP3, p-MLKL, and MLKL, as well as necrotic cell death after IVH; and (3) although Nec-1 treatment reduced microglial activation and the expression of inflammatory factors, this inhibitor had a limited effect on secondary hydrocephalus caused by IVH.

The majority of current adult IVH animal models use small rodents, such

as rats or mice. In previous reports, the IVH model in C57BL/6 mice was established using 25 μ L autologous blood for the lateral ventricular injections (Zhu et al., 2014a; Chen et al., 2019b). However, in this study, we found that when 23–27 g C57BL/6 mice were used for IVH modeling, injecting 50 μ L autologous blood into the lateral ventricle established a relatively stable IVH model without high mortality. We speculated that increasing the injection volume of autologous blood would induce greater pathological damage after IVH modeling, thereby producing more frequent complications after IVH, such as hydrocephalus, and aiding the study of brain damage caused by IVH. In this study, we confirmed the successful establishment of the IVH model using pathological tissue sections and T2-weighted MRI. Based on this model, we investigated whether necroptosis occurred after IVH induction and whether the necroptosis inhibitor Nec-1 provided neuroprotection.

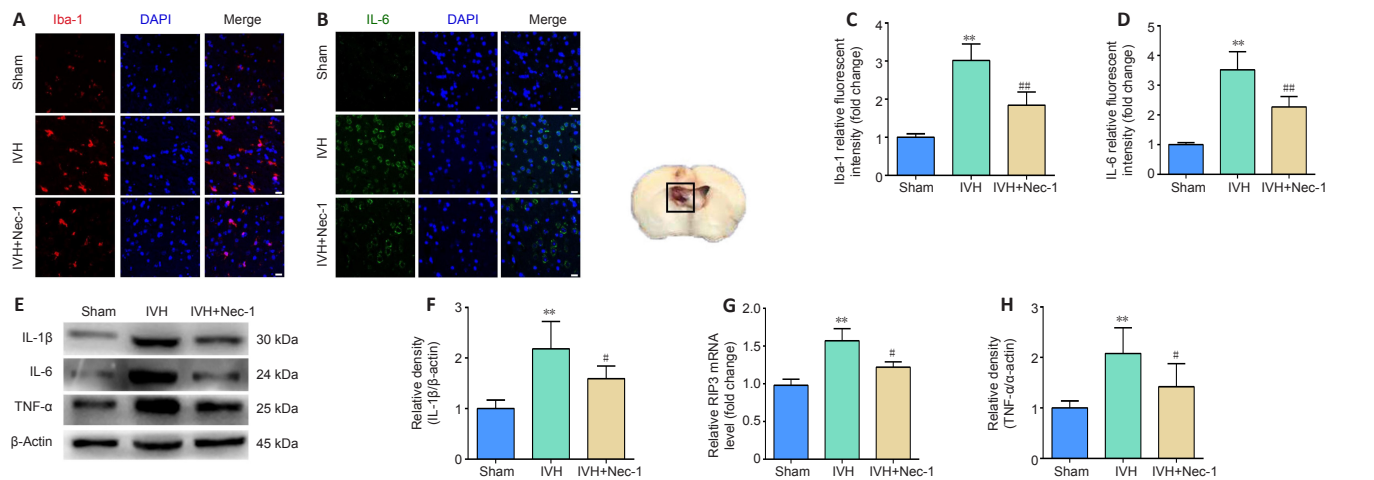


Figure 6 | Effects of necrostatin-1 on microglial activation and inflammation around the lateral ventricle after IVH induction.

(A) Representative images of Iba-1 (red, CoraLite594) immunofluorescent staining in the periventricular tissue. Compared with that in the sham group, the expression of Iba-1 was increased in the IVH group. Compared with that in the IVH group, Iba-1 expression decreased in the IVH + Nec-1 group. Scale bars: 20 μm. (B) Quantitative analyses of Iba-1 relative fluorescent intensities in the periventricular tissue. (C) Representative images of IL-6 (green, CoraLite488) immunofluorescent staining in the periventricular tissue. Compared with that in the sham group, the expression of IL-6 was increased in the IVH group. Compared with that in the IVH group, IL-6 expression decreased in the IVH + Nec-1 group. Scale bars: 20 μm. (D) Quantitative analyses of IL-6 relative fluorescent intensities in the periventricular tissue. (E) Representative western blots showing the protein expression of IL-1β, IL-6, and TNF-α. (F–H) Quantitative analyses of the changes in protein levels of IL-1β (F), IL-6 (G), and TNF-α (H). Data are expressed as the mean ± SEM (n = 6). **P < 0.01, vs. sham group; #P < 0.05, ###P < 0.01, vs. IVH group (unpaired Student's t-test). DAPI: 4',6-Diamidino-2-phenylindole; Iba-1: ionized calcium binding adapter molecule 1; IL: interleukin; IVH: intraventricular hemorrhage; Nec-1: necrostatin-1; TNF-α: anti-tumor necrosis factor-α.

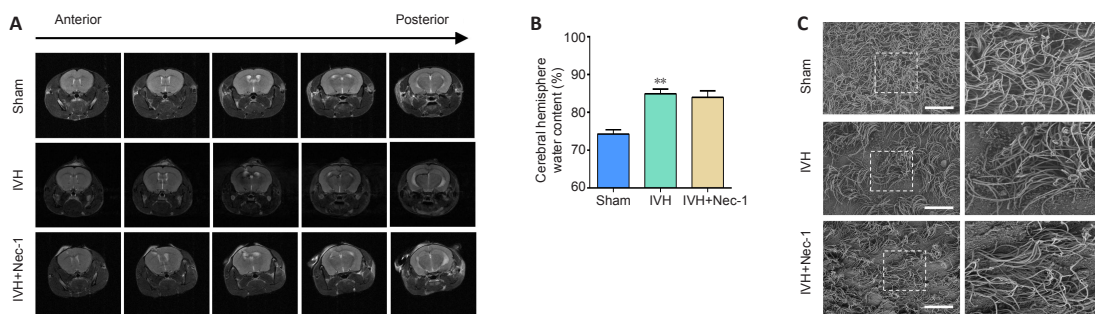


Figure 7 | Effects of necrostatin-1 on hydrocephalus after IVH induction.

(A) Representative images of T2 MRI scans. The sham group showed no hydrocephalus, while the IVH and IVH + Nec-1 groups showed significant hydrocephalus. (B) On day 3 after IVH induction, Nec-1 pretreatment did not significantly reduce the brain water content that was observed in the IVH only group. Data are expressed as the mean ± SEM (n = 3–6). **P < 0.01, vs. sham group (unpaired Student's t-test). (C) Scanning electron microscopy images showing the ependymal cilia. The ependymal cilia in the sham group were dense, while the ependymal cilia in IVH and IVH + Nec-1 groups were sparse and irregular. Scale bars: 10 μm. IVH: Intraventricular hemorrhage; MRI: magnetic resonance imaging; Nec-1: necrostatin-1.

Necroptosis is a newly discovered type of programmed cell death that is initiated by the tumor necrosis factor receptor and the Toll-like receptor families, regulated by RIP3 and MLKL, and manifests the characteristics of necrosis (Weinlich et al., 2017). Emerging studies have indicated that anti-necroptosis treatment promotes recovery from several central nervous system or related disorders, including subarachnoid hemorrhage, traumatic brain injury, and atherosclerosis (Karunakaran et al., 2016; Yuan et al., 2019b; Zhao et al., 2020). It has been reported that necroptosis is an important cell death method in ICH, and inhibition of necroptosis may be a potential strategy to improve the prognosis of ICH patients (Shen et al., 2017). At present, the detailed mechanism of cell death after IVH is unclear. In this study, we hypothesized that necroptosis would occur in the periventricular tissues of mice after IVH and inhibition of necroptosis may have a neuroprotective effect. A previous study demonstrated that the expression of RIP1 and RIP3 in the perihematoma tissues was highest on day 3 after ICH (Su et al., 2015). The current view is that the execution of necroptosis is dependent on RIP3 and MLKL (Yang et al., 2018). Therefore, RIP3, p-RIP3, p-MLKL and MLKL were the key necroptosis markers evaluated in this study. Similar to the results from the ICH model, the expression of RIP3 and MLKL increased and peaked on day 3 after IVH modeling. Immunohistochemistry confirmed that 3 days after IVH modeling, p-RIP3 and p-MLKL was increased in the periventricular tissues. After confirming the elevated expression of p-RIP3 and p-MLKL, it was important to explore the location of p-RIP3 and p-MLKL after IVH. Of note, previous studies have shown that necroptosis markers, such as RIP3, were mainly expressed in the neurons of mice with subarachnoid hemorrhage and ischemic stroke; however, there were no studies on the location of necroptosis markers after IVH (Chen et al., 2018; Hu et al., 2020). Our results showed that p-RIP3 and p-MLKL were mainly co-localized in neurons and rarely observed in astrocytes and microglia after IVH.

To further confirm whether the inhibition of necroptosis after IVH had a neuroprotective effect, Nec-1 was used. Nec-1 is known as a specific inhibitor

of RIP1 and can inhibit necroptosis (Degterev et al., 2008). At present, Nec-1 treatment has been shown to have neuroprotective effects after ischemic stroke and traumatic brain injury (Zhu et al., 2014b, 2021). Interestingly, recent studies indicated that Nec-1 treatment prevented an increase in hematoma volume after ICH (Chang et al., 2014). Whether Nec-1 exerted a neuroprotective effect by inhibiting necroptosis after IVH was unclear. Consistent with a previous study (You et al., 2008), our current study showed that Nec-1 decreased PI-positive cells after IVH. However, we found that Nec-1 treatment did not significantly alleviate periventricular and ependymal cilia injury.

Recent studies have revealed that either RIP3 deficiency or RIP1 inhibition may have therapeutic potential for tissue damage caused by inflammation and necroptosis (Patel et al., 2020; Zhang et al., 2020). Prior studies have shown that RIP3/MLKL-dependent necroptosis induced inflammation in a rat model of fluid percussion brain injury, while Nec-1 and GSK872 treatment inhibited the expression of pro-inflammatory cytokines (Liu et al., 2016). In addition, Nec-1 has been reported to suppress the RIP3/MLKL signaling pathway and have neuroprotective effects after subarachnoid hemorrhage by attenuating blood-brain barrier disruption and neuroinflammation (Chen et al., 2019a).

Microglia are resident immune cells in brain tissue that play a key role in neuroinflammation in many neurological diseases. The continued activation of microglia tends to trigger neuroinflammation, which exacerbates brain damage (Salter and Stevens, 2017). Therefore, in this study, we expected that necroptosis would have a pro-inflammatory effect after IVH, and Nec-1 treatment would effectively reduce inflammatory cytokine expression and microglial activation. Compared with that in the IVH only group, treatment with Nec-1 reduced the levels of pro-inflammatory cytokines and inhibited the activation of microglia. These results were consistent with our hypothesis. However, whether inhibition of pro-inflammatory cytokines through Nec-

1 treatment can reduce secondary hydrocephalus after IVH requires further investigation.

IVH can cause immediate obstructive hydrocephalus and delayed communicating hydrocephalus (Bu et al., 2016). Approximately 40% of adult patients with spontaneous ICH present with IVH, and the probability that this portion of patients suffer from hydrocephalus reaches 51–89% (Stein et al., 2010; Mustanoja et al., 2015). Current known mechanisms of hydrocephalus after IVH include alterations in the cerebrospinal fluid drainage pathway, ependyma, blood-brain barrier, aquaporin expression, inflammation, and degradation products of blood, such as iron (Mayfrank et al., 2000; Li et al., 2009; Strahle et al., 2012; Okubo et al., 2013). The IVH model established by injecting 200 µL of autologous blood into the lateral ventricle of rats can induce hydrocephalus 1 day after modeling, and hydrocephalus can be maintained for 14 days (Wan et al., 2020). In this study, we found secondary hydrocephalus on day 3 after IVH modeling in mice. Inflammation is a key factor in hydrocephalus, and our previous studies have shown that Nec-1 treatment can reduce the expression of inflammatory cytokines. In addition, as the ependyma is exposed to the blood itself or increased pressure, the surface of the ependyma is damaged (Sarnat, 1995; Simard et al., 2011). Defective ependymal cilia are thought to be an important mechanism for hydrocephalus, which can cause changes in the flow of cerebrospinal fluid (Ibañez-Tallon et al., 2004; Del Bigio, 2010). The results of scanning electron microscopy showed that the ependymal cilia were kinked, disorganized, and progressively lost after IVH, and Nec-1 treatment did not significantly reduce this damage. Although we found that Nec-1 alleviated necroptosis and inflammation, T2-weighted MRI showed that Nec-1 treatment appeared to have little effect on the degree of hydrocephalus after IVH. In other animal models of neurological disease (Chen et al., 2019a), the inhibition of necroptosis reduced the brain water content and the degree of hydrocephalus. Our study indicated that inhibition of necroptosis alone effectively inhibited the level of pro-inflammatory cytokines but not the degree of brain water content and hydrocephalus 3 days after IVH modeling in mice. This finding may indicate that simply inhibiting one type of cell death, such as necroptosis, has a limited effect on secondary hydrocephalus after IVH.

There were several limitations in this study. First, we observed changes in necroptosis markers from 1 to 7 days after IVH induction and did not explore whether there were changes in necroptosis markers in the longer term. Furthermore, treatment with different doses of Nec-1 may have alleviated long-term IVH-induced hydrocephalus. Second, Nec-1 has limitations, such as its moderate curative effect, and this inhibitor has off-target activity against indoleamine-2,3-dioxygenase as well as poor pharmacokinetic properties (Berger et al., 2015). In our study, we did not discuss how these limitations may have affected our results. Additionally, we only evaluated Nec-1 and did not use other necroptosis inhibitors, such as GSK963 and GSK872, to determine whether there was a neuroprotective effect after IVH induction in our model.

In conclusion, necroptosis occurred in periventricular tissues after IVH, and Nec-1 effectively inhibited the RIP3/MLKL-mediated necroptosis pathway, which alleviated necrotic cell death, neuroinflammation, and microglial activation in our model. However, Nec-1 treatment had little effect on IVH-induced hydrocephalus 3 days after modeling. Our study is the first to demonstrate a role for necroptosis after IVH induction and may provide new insight into novel therapeutic strategies to manage IVH.

Author contributions: *Study design: CL and YC; experiment implementation and manuscript drafting: HW and LZ; manuscript revising and modifying: KH and GWL; table and figure making: YXC, KRH and GQW; manuscript proposing and editing: LXZ and APT. All authors read and approved the final manuscript.*

Conflicts of interest: *The authors declare that there are no conflicts of interest associated with this manuscript.*

Availability of data and materials: *All data generated or analyzed during this study are included in this published article and its supplementary information files.*

Open access statement: *This is an open access journal, and articles are distributed under the terms of the Creative Commons AttributionNonCommercial-ShareAlike 4.0 License, which allows others to remix, tweak, and build upon the work non-commercially, as long as appropriate credit is given and the new creations are licensed under the identical terms.*

Open peer reviewers: *Faisal Alamri, King Saud bin Abdulaziz University for Health Sciences, Saudi Arabia.*

Additional file: *Open peer review report 1.*

References

Ballabh P, de Vries LS (2021) White matter injury in infants with intraventricular haemorrhage: mechanisms and therapies. *Nat Rev Neurol* 17:199-214.

Berger SB, Harris P, Nagilla R, Kasparcova V, Hoffman S, Swift B, Dare L, Schaeffer M, Capriotti C, Ouellette M, King BW, Wisnoski D, Cox J, Reilly M, Marquis RW, Bertin J, Gough PJ (2015) Characterization of GSK'963: a structurally distinct, potent and selective inhibitor of RIP1 kinase. *Cell Death Discov* 1:15009.

Bosche B, Mergenthaler P, Doeppner TR, Hescheler J, Molcanyi M (2020) Complex clearance mechanisms after intraventricular hemorrhage and rt-PA treatment—a review on clinical trials. *Transl Stroke Res* 11:337-344.

Bu Y, Chen M, Gao T, Wang X, Li X, Gao F (2016) Mechanisms of hydrocephalus after intraventricular haemorrhage in adults. *Stroke Vasc Neurol* 1:23-27.

Caccamo A, Branca C, Piras IS, Ferreira E, Huentelman MJ, Liang WS, Readhead B, Dudley JT, Spangenberg EE, Green KN, Belfiore R, Winslow W, Oddo S (2017) Necroptosis activation in Alzheimer's disease. *Nat Neurosci* 20:1236-1246.

Cao L, Mu W (2021) Necrostatin-1 and necroptosis inhibition: pathophysiology and therapeutic implications. *Pharmacol Res* 163:105297.

Chang P, Dong W, Zhang M, Wang Z, Wang Y, Wang T, Gao Y, Meng H, Luo B, Luo C, Chen X, Tao L (2014) Anti-necroptosis chemical necrostatin-1 can also suppress apoptotic and autophagic pathway to exert neuroprotective effect in mice intracerebral hemorrhage model. *J Mol Neurosci* 52:242-249.

Chen J, Jin H, Xu H, Peng Y, Jie L, Xu D, Chen L, Li T, Fan L, He P, Ying G, Gu C, Wang C, Wang L, Chen G (2019a) The neuroprotective effects of necrostatin-1 on subarachnoid hemorrhage in rats are possibly mediated by preventing blood-brain barrier disruption and RIP3-mediated necroptosis. *Cell Transplant* 28:1358-1372.

Chen T, Pan H, Li J, Xu H, Jin H, Qian C, Yan F, Chen J, Wang C, Chen J, Wang L, Chen G (2018) Inhibiting of RIPK3 attenuates early brain injury following subarachnoid hemorrhage: possibly through alleviating necroptosis. *Biomed Pharmacother* 107:563-570.

Chen W, Xia M, Guo C, Jia Z, Wang J, Li C, Li M, Tang X, Hu R, Chen Y, Liu X, Feng H (2019b) Modified behavioural tests to detect white matter injury-induced motor deficits after intracerebral haemorrhage in mice. *Sci Rep* 9:16958.

Degterev A, Huang Z, Boyce M, Li Y, Jagtap P, Mizushima N, Cuny GD, Mitchison TJ, Moskowitz MA, Yuan J (2005) Chemical inhibitor of nonapoptotic cell death with therapeutic potential for ischemic brain injury. *Nat Chem Biol* 1:112-119.

Degterev A, Hitomi J, Germscheid M, Ch'en IL, Korkina O, Teng X, Abbott D, Cuny GD, Yuan C, Wagner G, Hedrick SM, Gerber SA, Lugovskoy A, Yuan J (2008) Identification of RIP1 kinase as a specific cellular target of necrostatins. *Nat Chem Biol* 4:313-321.

Del Bigio MR (2010) Ependymal cells: biology and pathology. *Acta Neuropathol* 119:55-73.

Ding D, Starke RM, Dumont AS, Owens GK, Hasan DM, Chalouhi N, Medel R, Lin CL (2014) Therapeutic implications of estrogen for cerebral vasospasm and delayed cerebral ischemia induced by aneurysmal subarachnoid hemorrhage. *Biomed Res Int* 2014:727428.

Hanley DF, Lane K, McBee N, Ziai W, Tuhim S, Lees KR, Dawson J, Gandhi D, Ullman N, Mould WA, Mayo SW, Mendelow AD, Gregson B, Butcher K, Vespa P, Wright DW, Kase CS, Carhuapoma JR, Keyl PM, Diener-West M, et al. (2017) Thrombolytic removal of intraventricular haemorrhage in treatment of severe stroke: results of the randomised, multicentre, multiregion, placebo-controlled CLEAR III trial. *Lancet* 389:603-611.

Hu W, Wu X, Yu D, Zhao L, Zhu X, Li X, Huang T, Chu Z, Xu Y (2020) Regulation of JNK signaling pathway and RIP3/AIF in necroptosis-mediated global cerebral ischemia/reperfusion injury in rats. *Exp Neurol* 331:113374.

Ibañez-Tallon I, Pagenstecher A, Fliegau M, Olbrich H, Kispert A, Ketelsen UP, North A, Heintz N, Omran H (2004) Dysfunction of axonemal dynein heavy chain Mdnah5 inhibits ependymal flow and reveals a novel mechanism for hydrocephalus formation. *Hum Mol Genet* 13:2133-2141.

Jabbarli R, Reinhard M, Roelz R, Shah M, Niesen WD, Kaier K, Taschner C, Weyerbrock A, Velthoven VV (2016) The predictors and clinical impact of intraventricular hemorrhage in patients with aneurysmal subarachnoid hemorrhage. *Int J Stroke* 11:68-76.

Karunakaran D, Geoffrion M, Wei L, Gan W, Richards L, Shangari P, DeKemp EM, Beanlands RA, Perisic L, Maegdefessel L, Hedin U, Sad S, Guo L, Kolodgie FD, Virmani R, Ruddy T, Rayner KJ (2016) Targeting macrophage necroptosis for therapeutic and diagnostic interventions in atherosclerosis. *Sci Adv* 2:e1600224.

Klebe D, McBride D, Krafft PR, Flores JJ, Tang J, Zhang JH (2020) Posthemorrhagic hydrocephalus development after germinal matrix hemorrhage: Established mechanisms and proposed pathways. *J Neurosci Res* 98:105-120.

- Ko HR, Ahn SY, Chang YS, Hwang I, Yun T, Sung DK, Sung SI, Park WS, Ahn JY (2018) Human UCB-MSCs treatment upon intraventricular hemorrhage contributes to attenuate hippocampal neuron loss and circuit damage through BDNF-CREB signaling. *Stem Cell Res Ther* 9:326.
- Kowalski RG, Hammond FM, Weintraub AH, Nakase-Richardson R, Zafonte RD, Whyte J, Giacino JT (2021) Recovery of consciousness and functional outcome in moderate and severe traumatic brain injury. *JAMA Neurol* 78:548-557.
- Li X, Kong H, Wu W, Xiao M, Sun X, Hu G (2009) Aquaporin-4 maintains ependymal integrity in adult mice. *Neuroscience* 162:67-77.
- Liang YX, Wang NN, Zhang ZY, Juan ZD, Zhang C (2019) Necrostatin-1 ameliorates peripheral nerve injury-induced neuropathic pain by inhibiting the RIP1/RIP3 pathway. *Front Cell Neurosci* 13:211.
- Liu T, Zhao DX, Cui H, Chen L, Bao YH, Wang Y, Jiang JY (2016) Therapeutic hypothermia attenuates tissue damage and cytokine expression after traumatic brain injury by inhibiting necroptosis in the rat. *Sci Rep* 6:24547.
- Mayfrank L, Kim Y, Kissler J, Delsing P, Gilsbach JM, Schröder JM, Weis J (2000) Morphological changes following experimental intraventricular haemorrhage and intraventricular fibrinolytic treatment with recombinant tissue plasminogen activator. *Acta Neuropathol* 100:561-567.
- Morrice JR, Gregory-Evans CY, Shaw CA (2017) Necroptosis in amyotrophic lateral sclerosis and other neurological disorders. *Biochim Biophys Acta Mol Basis Dis* 1863:347-353.
- Moullaali TJ, Sato S, Wang X, Rabinstein AA, Arima H, Carcel C, Chen G, Robinson T, Heeley E, Chan E, Delcourt C, Stapf C, Cordonnier C, Lindley RI, Chalmers J, Anderson CS (2017) Prognostic significance of delayed intraventricular haemorrhage in the INTERACT studies. *J Neurol Neurosurg Psychiatry* 88:19-24.
- Mustanoja S, Satopää J, Meretoja A, Putaala J, Strbian D, Curtze S, Haapaniemi E, Sairanen T, Niemelä M, Kaste M, Tatlisumak T (2015) Extent of secondary intraventricular hemorrhage is an independent predictor of outcomes in intracerebral hemorrhage: data from the Helsinki ICH Study. *Int J Stroke* 10:576-581.
- Naito MG, Xu D, Amin P, Lee J, Wang H, Li W, Kelliher M, Pasparakis M, Yuan J (2020) Sequential activation of necroptosis and apoptosis cooperates to mediate vascular and neural pathology in stroke. *Proc Natl Acad Sci U S A* 117:4959-4970.
- Okubo S, Strahle J, Keep RF, Hua Y, Xi G (2013) Subarachnoid hemorrhage-induced hydrocephalus in rats. *Stroke* 44:547-550.
- Patel S, Webster JD, Varfolomeev E, Kwon YC, Cheng JH, Zhang J, Dugger DL, Wickliffe KE, Maltzman A, Sujatha-Bhaskar S, Bir Kohli P, Ramaswamy S, Deshmukh G, Liederer BM, Fong R, Hamilton G, Lupardus P, Caplazi P, Lee WP, van Lookeren Campagne M, et al. (2020) RIP1 inhibition blocks inflammatory diseases but not tumor growth or metastases. *Cell Death Differ* 27:161-175.
- Percie du Sert N, Hurst V, Ahluwalia A, Alam S, Avey MT, Baker M, Browne WJ, Clark A, Cuthill IC, Dirnagl U, Emerson M, Garner P, Holgate ST, Howells DW, Karp NA, Lázic SE, Lidster K, MacCallum CJ, Macleod M, Pearl EJ, et al. (2020) The ARRIVE guidelines 2.0: Updated guidelines for reporting animal research. *PLoS Biol* 18:e3000410.
- Salter MW, Stevens B (2017) Microglia emerge as central players in brain disease. *Nat Med* 23:1018-1027.
- Sarnat HB (1995) Ependymal reactions to injury. A review. *J Neuropathol Exp Neurol* 54:1-15.
- Schneider CA, Rasband WS, Eliceiri KW (2012) NIH Image to ImageJ: 25 years of image analysis. *Nat Methods* 9:671-675.
- Segado-Arenas A, Infante-García C, Benavente-Fernández I, Sánchez-Sotano D, Ramos-Rodríguez JJ, Alonso-Ojembarrena A, Lubian-Lopez S, Garcia-Alloza M (2018) Cognitive impairment and brain and peripheral alterations in a murine model of intraventricular hemorrhage in the preterm newborn. *Mol Neurobiol* 55:4896-4910.
- Shen H, Liu C, Zhang D, Yao X, Zhang K, Li H, Chen G (2017) Role for RIP1 in mediating necroptosis in experimental intracerebral hemorrhage model both in vivo and in vitro. *Cell Death Dis* 8:e2641.
- Simard PF, Tosun C, Melnichenko L, Ivanova S, Gerzanich V, Simard JM (2011) Inflammation of the choroid plexus and ependymal layer of the ventricle following intraventricular hemorrhage. *Transl Stroke Res* 2:227-231.
- Stein M, Luecke M, Preuss M, Boeker DK, Joedicke A, Oertel MF (2010) Spontaneous intracerebral hemorrhage with ventricular extension and the grading of obstructive hydrocephalus: the prediction of outcome of a special life-threatening entity. *Neurosurgery* 67:1243-1251; discussion 1252.
- Strahle J, Garton HJ, Maher CO, Muraszko KM, Keep RF, Xi G (2012) Mechanisms of hydrocephalus after neonatal and adult intraventricular hemorrhage. *Transl Stroke Res* 3:25-38.
- Su X, Wang H, Kang D, Zhu J, Sun Q, Li T, Ding K (2015) Necrostatin-1 ameliorates intracerebral hemorrhage-induced brain injury in mice through inhibiting RIP1/RIP3 pathway. *Neurochem Res* 40:643-650.
- Wallach D, Kang TB, Dillon CP, Green DR (2016) Programmed necrosis in inflammation: Toward identification of the effector molecules. *Science* 352:aaf2154.
- Wan Y, Gao F, Ye F, Yang W, Hua Y, Keep RF, Xi G (2020) Effects of aging on hydrocephalus after intraventricular hemorrhage. *Fluids Barriers CNS* 17:8.
- Weinlich R, Oberst A, Beere HM, Green DR (2017) Necroptosis in development, inflammation and disease. *Nat Rev Mol Cell Biol* 18:127-136.
- Yang J, Zhao Y, Zhang L, Fan H, Qi C, Zhang K, Liu X, Fei L, Chen S, Wang M, Kuang F, Wang Y, Wu S (2018) RIPK3/MLKL-mediated neuronal necroptosis modulates the M1/M2 polarization of microglia/macrophages in the ischemic cortex. *Cereb Cortex* 28:2622-2635.
- You Z, Savitz SI, Yang J, Degterev A, Yuan J, Cuny GD, Moskowitz MA, Whalen MJ (2008) Necrostatin-1 reduces histopathology and improves functional outcome after controlled cortical impact in mice. *J Cereb Blood Flow Metab* 28:1564-1573.
- Yuan J, Amin P, Ofengeim D (2019a) Necroptosis and RIPK1-mediated neuroinflammation in CNS diseases. *Nat Rev Neurosci* 20:19-33.
- Yuan S, Yu Z, Zhang Z, Zhang J, Zhang P, Li X, Li H, Shen H, Chen G (2019b) RIP3 participates in early brain injury after experimental subarachnoid hemorrhage in rats by inducing necroptosis. *Neurobiol Dis* 129:144-158.
- Zhang Y, Li M, Li X, Zhang H, Wang L, Wu X, Zhang H, Luo Y (2020) Catalytically inactive RIP1 and RIP3 deficiency protect against acute ischemic stroke by inhibiting necroptosis and neuroinflammation. *Cell Death Dis* 11:565.
- Zhao P, Li C, Chen B, Sun G, Chao H, Tu Y, Bao Z, Fan L, Du X, Ji J (2020) Up-regulation of CHMP4B alleviates microglial necroptosis induced by traumatic brain injury. *J Cell Mol Med* 24:8466-8479.
- Zhu W, Gao Y, Chang CF, Wan JR, Zhu SS, Wang J (2014a) Mouse models of intracerebral hemorrhage in ventricle, cortex, and hippocampus by injections of autologous blood or collagenase. *PLoS One* 9:e97423.
- Zhu X, Park J, Golinski J, Qiu J, Khuman J, Lee CC, Lo EH, Degterev A, Whalen MJ (2014b) Role of Akt and mammalian target of rapamycin in functional outcome after concussive brain injury in mice. *J Cereb Blood Flow Metab* 34:1531-1539.
- Zhu YM, Lin L, Wei C, Guo Y, Qin Y, Li ZS, Kent TA, McCoy CE, Wang ZX, Ni Y, Zhou XY, Zhang HL (2021) The key regulator of necroptosis, RIP1 kinase, contributes to the formation of astrogliosis and glial scar in ischemic stroke. *Transl Stroke Res* 12:991-1017.

P-Reviewer: Alamri F; C-Editor: Zhao M; S-Editors: Yu J, Li CH; L-Editors: Zunino S, Yu J, Song LP; T-Editor: Jia Y